
This is an electronic reprint of the original article.
This reprint may differ from the original in pagination and typographic detail.

Dimic-Misic, Katarina; Buffiere, Jean; Imani, Monireh; Nieminen, Kaarlo; Sixta, Herbert; Gane, Patrick

Improved stabilisation of graphite nanoflake dispersions using hydrothermally-produced nanocellulose

Published in:
Colloids and Surfaces A: Physicochemical and Engineering Aspects

DOI:
[10.1016/j.colsurfa.2020.125668](https://doi.org/10.1016/j.colsurfa.2020.125668)

Published: 05/02/2021

Document Version
Peer-reviewed accepted author manuscript, also known as Final accepted manuscript or Post-print

Published under the following license:
CC BY-NC-ND

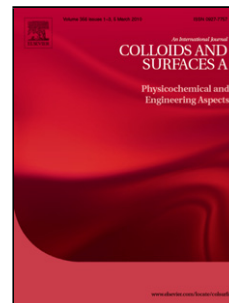
Please cite the original version:
Dimic-Misic, K., Buffiere, J., Imani, M., Nieminen, K., Sixta, H., & Gane, P. (2021). Improved stabilisation of graphite nanoflake dispersions using hydrothermally-produced nanocellulose. *Colloids and Surfaces A: Physicochemical and Engineering Aspects*, 610, Article 125668. <https://doi.org/10.1016/j.colsurfa.2020.125668>

This material is protected by copyright and other intellectual property rights, and duplication or sale of all or part of any of the repository collections is not permitted, except that material may be duplicated by you for your research use or educational purposes in electronic or print form. You must obtain permission for any other use. Electronic or print copies may not be offered, whether for sale or otherwise to anyone who is not an authorised user.

Journal Pre-proof

Improved stabilisation of graphite nanoflake dispersions using hydrothermally-produced nanocellulose

Katarina Dimic-Misic, Jean Buffiere, Monireh Imani, Kaarlo Nieminen, Herbert Sixta, Patrick Gane



PII: S0927-7757(20)31261-9

DOI: <https://doi.org/10.1016/j.colsurfa.2020.125668>

Reference: COLSUA 125668

To appear in: *Colloids and Surfaces A: Physicochemical and Engineering Aspects*

Received Date: 28 July 2020

Revised Date: 23 September 2020

Accepted Date: 23 September 2020

Please cite this article as: Dimic-Misic K, Buffiere J, Imani M, Nieminen K, Sixta H, Gane P, Improved stabilisation of graphite nanoflake dispersions using hydrothermally-produced nanocellulose, *Colloids and Surfaces A: Physicochemical and Engineering Aspects* (2020), doi: <https://doi.org/10.1016/j.colsurfa.2020.125668>

This is a PDF file of an article that has undergone enhancements after acceptance, such as the addition of a cover page and metadata, and formatting for readability, but it is not yet the definitive version of record. This version will undergo additional copyediting, typesetting and review before it is published in its final form, but we are providing this version to give early visibility of the article. Please note that, during the production process, errors may be discovered which could affect the content, and all legal disclaimers that apply to the journal pertain.

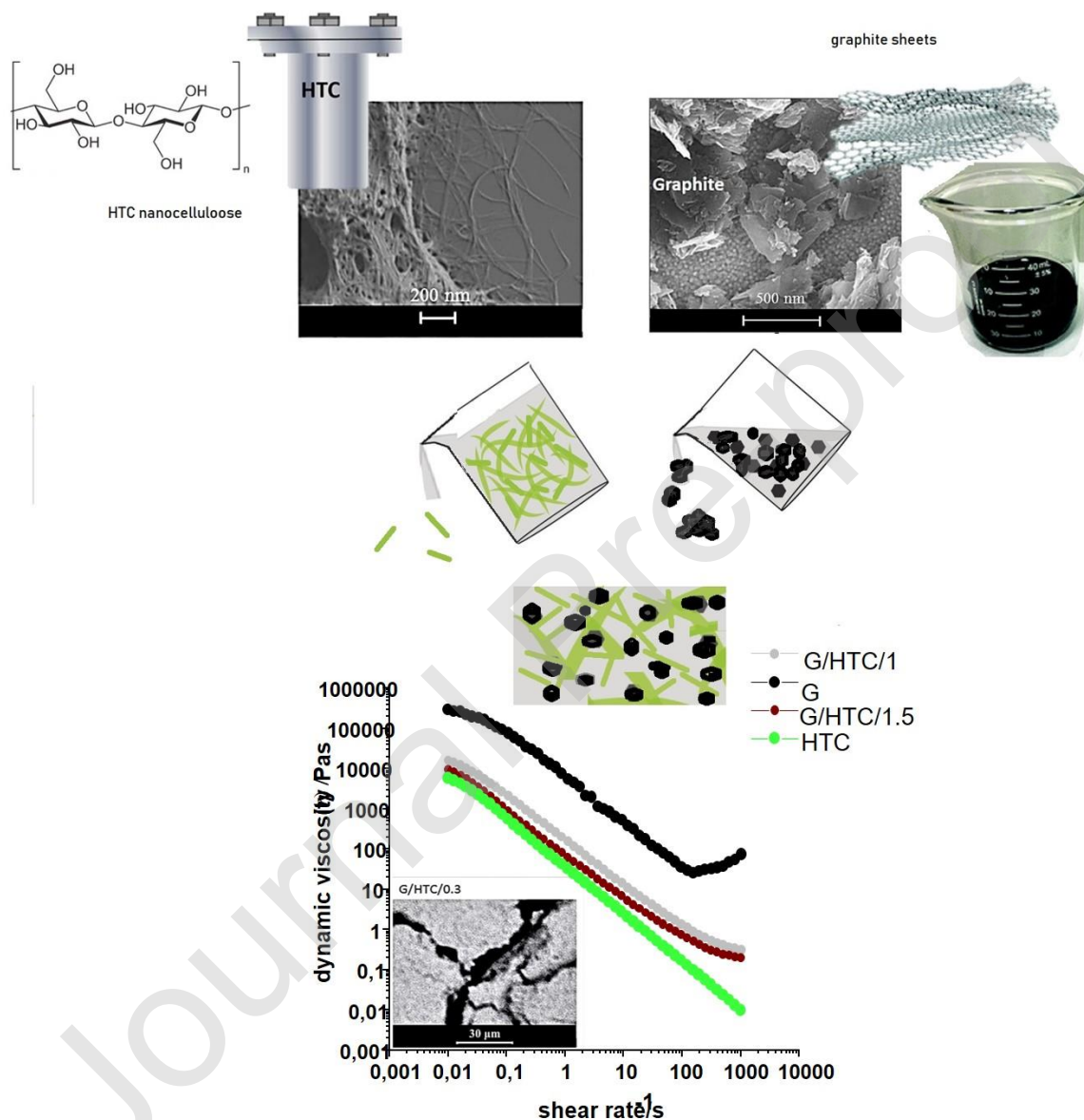
© 2020 Published by Elsevier.

Improved stabilisation of graphite nanoflake dispersions using hydrothermally-produced nanocellulose

Katarina Dimic-Misic, Jean Buffiere, Monireh Imani, Kaarlo Nieminen, Herbert Sixta, Patrick Gane

School of Chemical Engineering, Department of Bioproducts and Biosystems, P.O. Box 16300, Aalto University, FI-00076 Aalto, Helsinki, Finland

Graphical abstract



HIGHLIGHTS:

- Hydrothermally-produced nanocellulose was used as aqueous nanographite dispersant
- Nanocellulose showed higher total surface energy and favorable morphology
- Two-fold improvement in aggregate size reduction prevented graphite agglomeration
- Nanocellulose-nanographite mixture also retained desirable thixotropic behavior
- Results confirm advantage of such nanocellulose for aqueous exfoliation to graphene

Abstract

Dispersing graphite nanopflakes in aqueous suspension is essential both during their processing and to realise the high level of functionality they offer. In this study two types of chemical-free nanocelluloses were assessed as possible dispersing agent for graphite nanoflakes. Hydrothermally-produced nanocellulose (HTC) obtained by supercritical water treatment of microcrystalline cellulose, showed superior dispersing than the more conventional, mechanically-produced microfibrillated nanocellulose (MFC) alternative, effectively preventing nanoflake agglomeration. Thanks to the specific processing method, the HTC material displayed higher total surface energy and a favourable particle morphology. These properties resulted in a 2-fold reduction in the volume median colloidal particle size of nanographite in suspension upon addition of only 2 w/w% nanocellulose. The improved single particle dispersion within the suspension matrix could be observed microscopically and was reflected rheologically. The latter was achieved by parameterising the stress-shear rate response and fitting the linear segments displaying the suspension coupling response. Using chemical-free nanocellulose as dispersant in aqueous medium is a positive step toward the exfoliation of nanographite into graphene in a more affordable and environmentally-friendly way.

Keywords: nanographite, nanocellulose, supercritical water, nanoparticle dispersion, green chemistry

1. INTRODUCTION

Nanocellulose and nanocellulosic composites are finding wide-ranging application in many advanced industries. In-roads have been made particularly in speciality materials, and in fields such as medical and electronics, due mainly to their excellent mechanical, barrier and biodegradable properties [1]. Nanocellulose-containing composite properties can be enhanced through the addition of particulate functional fillers, including silica, calcium carbonate, nanoclays and specialised fibre components to enhance stiffness, toughness, hardness, resistance to heat distortion and also significant processing cost reduction [2]. One of the most interesting areas for enhancement is the combination with electrically conductive and mechanically enhancing graphite nanoparticles [3]. The extent of improvement, however, is strongly dependent on the combined processing method, filler concentration, morphology and, highly significantly, on the interfacial compatibility with the cellulose fibrils in aqueous suspension [4]. Carbon materials (including graphite, carbon nanotubes and graphene) are obvious candidates also for reinforcement to develop multifunctional engineering components combining high mechanical performance and reliability. Graphite nanomaterials are increasingly sought after for use in fabricating various micro-electrical devices, batteries, supercapacitors, and composites. Optimum properties are, therefore, ultimately controlled by the state of compatibility with water within the nanocellulose gel-like matrix during processing and prior to consolidation and drying [2,5].

The problem of poor aqueous dispersion is generally encountered during the addition of increasing functional filler concentration, for example to enhance conductivity in the case of graphite nanoflakes, which results in property inhomogeneity and processing difficulties related to agglomeration of the functional phase and distortion of uniformity of the nanocellulose matrix [5,6]. In comparison to graphene, graphite, in turn, presents the much less costly filler among carbon allotropes, decreasing manufacturing cost of composite materials [4]. Reason for that is that their presence whether as a part of coating or a reinforcement in composites filler particles, provides for novel products excellent thermal [7,8] and electrical conductivity [9–11]. When mechanical properties are also sought for,

graphite flakes used as filler reinforcement also improve friction resistance, seizure (a major problem associated with the use of metals when under mechanical stress) and reduced wear behaviour [12,13]. Carbon atoms on the graphite surface have aromatic bonds and this makes them chemically stable, such as in the case of graphite layers packed in sheets which are bound by van der Waals forces. This inevitably leads to a drastic aggregation of the graphite nanoflakes, which gives rise to the generally found poor long-term colloidal stability of non-oxidised graphene when preparing such water based nanocomposites [14].

The development of robust but lightweight composite materials with high mechanical strength, low wear, low seizure tendency, and low electrical loss, as described above, are of paramount importance also amongst advances supporting environmental and resulting societal change [4,5]. However, industrial production of such composite materials remains expensive and is still limited to fundamental research and used only for high end specific applications [13].

Natural graphite flakes are a direct source of high-quality pure material for potential processing into graphene through either mechanical exfoliation or liquid-phase exfoliation of fine powders. In such processes, chemicals such as aromatic compounds, certain surfactants, polymers, and even carbon quantum dots, are used, to prevent aggregation and restacking in the production of nanographite composites [15]. However, despite the hydrodynamic forced contact between the graphite nanoflakes, these additives remain on the particle surface, having both a negative environmental impact and decreasing the electrical performance of the resulting composite [15,16]. Furthermore, organic solvents cannot be applied if the product is aimed at use in water-soluble cellulosic polymer composites, where wetting and biocompatibility are necessary, such as in drug loading and delivery, tissue engineering or green chemistry

Micro-nanofibrillar cellulose has shown to be a suitable dispersant of graphite flakes in the mechanical exfoliation process, where shearing forces enabled close contact and penetration of fibrils within agglomerated graphite flakes that promoted delamination into graphene, this producing graphene-cellulose composite [17–19]. The target remains to continue to improve the dispersing power of nanocellulose for graphite-derived nanoparticles further, and this paper reports on a major step in this direction starting from microcrystalline cellulose (MCC).

An odourless, tasteless and relatively inert compound, MCC is a relatively pure form of cellulose that is readily available commercially, produced by a moderate hydrolysis of pulp using mineral acids, such as hydrochloric acid or sulphuric acid [1,2,20]. While acidic conditions trigger the complete hydrolysis of hemicelluloses contained in the starting wood pulp, the regions of the cellulosic fibres with weaker long-range order are also hydrolysed down to the so-called level-off degree of polymerisation (DP) [21,22]. Once dried, the resulting powder has a typical particle size between 20 and 100 μm , and, as such, has found use as a thickener, emulsifier, wet granulation excipient finding increasing use in the food and pharmaceutical industries [23,24].

MCC has been also used as a relevant starting point for further mechanical size reduction of cellulose. As an alternative, near-critical and supercritical water treatments of MCC, whereby MCC is mixed with pure water under elevated temperatures and pressures in the vicinity or above its critical point (374 °C and 22.1 MPa) respectively, trigger the near instantaneous hydrolysis of cellulose chains degrading them to a complex mixture of oligomers and low-molecular-weight cellulose [25,26]. This specific reactivity is due to the combination of high reaction temperatures and the unique properties of near-critical and supercritical water, such as reduced density, polarity and heat conductivity [27,28]. Under such treatment short oligomers essentially remain water-soluble whilst the longer chains, however, precipitate into a white solid material that can be recovered after the treatment [29]. This novel material has a high crystallinity index and has been demonstrated that can be used as a Pickering stabiliser for oil-in-water emulsions thanks to the high aspect ratio and high total surface energy of its particles [30]. In addition, the presence of polar OH and CH functional groups enables the

hydrophilicity and hydrophobicity of cellulose to be adjusted through chemical surface modification [29,30].

Blends of microfibrillated cellulose and graphene were successfully prepared as a first step to building functional composite materials with electromagnetic properties, forming flexible composite films composed of graphene and microfibrillated cellulose (MFC) and/or cellulose nanofibrils (CNF) by co-exfoliation of graphite in MFC suspension using high-shear forces [31,32]. The amphiphilic nature of cellulose fibres enables them to act as both dispersing and homogenising agent while graphite nanoflakes dispersed in this way retain their partial hydrophobicity, that results in a complex rheological behaviour such particles coupling in a shear gradient [33,34]. Good dispersion of graphite nanoflakes, which have been observed to have peculiar rheological behaviours, such as strain hardening and dilatant thixotropic behaviour, into biomaterials with high surface area, is beneficial for the preparation of graphite composites [35–40].

This work uses a comparative approach between two the differently produced cellulose materials MFC and HTC to illustrate the improved dispersing power of HTC, whilst simultaneously adding to the knowledge gained in a previous study of preparation of graphene-MFC composites by dispersion and exfoliation of graphite in MFC [33,34]. The hypothesis of this research was based on the assumption that the specific surface properties of nanocellulose produced from hydrothermal treatment (HTC) can be suitable for mitigating the dispersive surface energy of graphite nanoflakes, ultimately rendering the dispersion hydrophilic [37,40]. To reveal this effect on graphite nanoflake dispersion, and understanding their rheological response in both viscoelastic and dynamic conditions [37,41], rheological and morphological analyses, together with surface property measurements, were applied as tools to examine the comparative influence of the two different types of nanocellulose, with their contrasting morphology and surface chemistry.

2. MATERIALS AND METHODS

2.1 Preparation of MFC from high-pressure homogenisation

MFC was prepared from the commercial MCC named Avicel PH-101 (Sigma Aldrich, Germany) with a high-pressure homogeniser Microfluidizer® M-110P (Microfluidics Corp., Westwood, MA, USA) that consists of two Y-shaped impact chambers connected in series, as described by Vanhatalo *et al.* [23]. MCC was mixed with deionised (DI) water from an ion-exchange system (Pureflow Inc, NC, USA) with a conductivity below $1.0 \mu\text{S}\cdot\text{cm}^{-1}$, to a consistency of 15 w/w%, then diluted to a consistency of 4.5 w/w%, with a pH of 5.5. This was defined experimentally as the maximum consistency that would not cause clogging within flow channels. The production pressure was 20 MPa, internal diameter of the first impact chamber flow channel was 200 μm and the second 100 μm . The size reduction of MCC particles down to nanoscale fibril-containing MFC suspensions was achieved with 5 passes at room temperature (20 °C), until a material with the desired rheological properties was obtained [24].

2.2 Production of HTC from supercritical water treatment

HTC was produced alternatively from a commercial comparative MCC (Merck, Germany) using a supercritical water reactor setup described in detail by Buffiere *et al.* [29,30]. In short, a 1.0 w/w% MCC suspension in cold water (20 °C) was pressurised to 25 MPa and mixed with supercritical water (520 °C) at the one end of a tubular reactor. This brought the mixture to a temperature of $395 \text{ °C} \pm 1 \text{ °C}$ and initiated the depolymerisation and dissolution of MCC. The mixture was cooled down at the other end of the reactor by addition of cold liquid water (20 °C), which brought the temperature of the mixture down to around 270 °C and stopped the reaction. The total reactor length was 52 mm corresponding to a total reaction time of approximately 60 ms. The product then flowed through a heat exchanger for further cooling down a back-pressure regulator to depressurisation before recovery and sampling. After settling for 48 h at temperature of 4 °C, centrifugation (Eppendorf,

Germany) at 10 000 min⁻¹ (rpm) for 20 min was used to separate solid and liquid fractions. The recovered material had a dry matter content of 15 w/w%.

2.3 Preparation of graphite-nanocellulose suspensions

Graphite nanoflakes were supplied by Asbury Carbons (GNP 307 supplied by Asbury Carbons, NJ, USA). Following earlier work using MFC to aid mechanical co-exfoliation of graphite to graphene-MFC suspensions the SCAN-P-55:88 method was used for evaluating the quantity of dispersing agent in suspension in relation to pigment particles [33]. The ratio of graphite in suspensions is hereby referred to as “G”. A paste of 15 w/w% graphite nanoflakes in water was prepared as initial suspension that was capable of good mixing, and diluted to 8 w/w%, which proved to be the minimum consistency that allowed for uniform paste-like material. HTC/MFC suspensions were diluted with deionised water, to 15 w/w% (later 8 w/w%) and 4 w/w%, respectively. Sonication of vessels with suspensions was applied in a water bath at ambient room temperature to maintain constant temperature using a Hielscher UIP1000hd (Germany) ultrasonication probe at a power output of 60 W for 6 min. Keeping constant volume ratio between graphite flakes dispersion of 8 w/w% and either HTC or MFC within 4 w/w% suspensions, different suspensions of graphite nanoflakes and addition of either MFC or HTC (MFC/HTC). The final graphite/nanocellulose mixture always consisted of 5 parts, i.e. 3 parts of 8 w/w% graphite/water suspension, and another 2 parts, which initially comprises pure water, which in turn was then gradually replaced with increasing amounts of 4 w/w% nanocellulose suspension (Fig. 2). Conversion from “parts” to mass content is shown in Table 1. Complex suspensions of graphite flakes and nanocellulose were mixed under high shear for 10 min using an Ultra-Turrax mixer, with rotation speed of 13 000 min⁻¹ (rpm), so that the essentially one-dimensional rod structure of cellulose could enter between the two-dimensional graphite flakes and form a uniform stable suspension and hydrogel. The pH in the aqueous suspensions was controlled and adjusted to 7, both before and after mixing HTC or MFC with the graphite nanoflakes.

Table 1. MFC and HTC produced dispersants and their colloidal dispersing combinations with graphite nanoflakes, G.

Samples: 5 parts of suspension	MFC/HTC (4 w/w%) suspension / parts	G (8 w/w%) suspension / parts	MFC/HTC amount in suspension / g	G amount in suspension / g	MFC/HTC consistency in suspension / w/w%	G consistency in suspension / w/w%	Total mass of suspension / g	Total solids in suspension [G/MFC/HTC] / w/w%
G	0	3.0	0	37.5	0	8.00	37.5	8.00
G/MFC/HTC/0.1	0.10	3.0	2.5	37.5	0.25	7.50	40.0	7.75
G/MFC/HTC/0.3	0.30	3.0	7.5	37.5	0.67	6.67	45.0	7.33
G/MFC/HTC/0.5	0.50	3.0	12.5	37.5	1.00	6.00	50.0	7.00
G/MFC/HTC/1.0	1.00	3.0	25.0	37.5	1.14	3.43	87.5	4.57
G/MFC/HTC/1.5	1.50	3.0	37.5	37.5	2.00	4.00	75.0	6.00
G/MFC/HTC/2.0	2.00	3.0	50.0	37.5	2.29	3.43	87.5	5.71

2.5 Rheology of suspensions

All rheological measurements were obtained with plate-plate geometry with serrated surface profile on both upper and lower plates to avoid apparent wall-slip due to sample solids depletion. Measurements were made on an MCR 302 rheometer (Anton Paar, Graz, Austria). The upper plate diameter was 20 mm with gap setting of 1.3 mm. The bottom plate was set via Peltier temperature control to a constant temperature of 23 °C. All suspensions were measured five times, with a new

sample used prior to each recording of data. Prior to measurements all samples were pre-sheared at constant shear rate of 100 s^{-1} for 60 s, and then left to rest for a further 60 s to allow for identical stress within highly viscoelastic suspensions, thus avoiding a "memory time effect" [24]. Data variation was within 10 %, due to the thixotropy of suspensions, as observed earlier for similar systems [34].

In order to be able to upscale laboratory results to production facilities, suspensions have to be handled identically prior to measurements. This is especially important for nanocellulose liquid hydrogels, at consistency higher than 1.5 w/w% [40, 42]. Concentrated particulate gels with complex interactions between particles are particle jammed systems, such that they are mechanically pasty materials with a yield stress, which needs to be exceeded beyond its critical static stress, τ_s^0 , such that the suspension can be made to begin to flow. Steady state paste materials, as such, continue to flow if the applied shear stress is maintained larger than this critical value. If during shear the stress falls below the fully developed dynamic stress limit throughout the sample, τ_d^0 , the material starts to develop quasi-static conditions. For such materials the interface between the non-sheared and sheared regions is complex due to non-uniform distribution of stress within the suspension, and they become susceptible to phase separation and thus apparent wall slippage and shear banding. Such systems cannot be defined with respect to settlement rate after pre-shearing and rest time [43]. Therefore, shear banding, apparent wall slip and settling are always present in such non-linear systems, and such effects may typically contribute to $\sim 10 \%$ response variation. However, high aspect ratio laminar materials at such ultrafine size as considered here undergo Brownian motion, which acts to randomise position and, as such, acts against any significant settling/sedimentation. Nonetheless, primarily for reasons of likely phase separation, each measurement was repeated five times, each time taking a new sample [43–45].

Noise reduction in the raw data was additionally applied using a correction process in which primarily negative values and values off-scale were removed. The data were then processed using a Tikhonov regularisation step, which consists of minimising to a localised linear combination of results and provides a term representing the amount of remaining noise in the smoothed data [40]. Fitting low order polynomials to the ends of the data and replacing the y -coordinate values of the ends with values calculated from these fits, prevent the appearance of unnecessary winding. Adjusting segmentally the ratio between the coefficients in the residual amount between raw and smoothed data determines the level of smoothness.

2.5.1 Shear response

Flow curves were measured as a function of logarithmically increasing shear rate within a four decades shear rate range ($\dot{\gamma} = 0.01 - 1\,000 \text{ s}^{-1}$), with a logarithmic spread of data point, duration ranging from 100 to 1 s to attain equilibrium on strain imposed on sample.

The Ostwald-de Waele expression for purely viscous shear thinning is given by Eq. (1)

$$\eta = k\dot{\gamma}^{n-1} \quad (1)$$

used to fit the thixotropic shear response behaviour, where k and n are the consistency and power-law index, respectively, and $\dot{\gamma}$ is the shear rate [38,46,47].

2.5.2 Viscoelastic rheological measurements

Oscillatory measurement began with an amplitude sweep, applying strain (γ) across the range between 0.1 and 1 000 %, maintaining a constant angular frequency (ω) of 1 (rad)s^{-1} , to determine the quasi-linear viscoelastic region (LVE) [24,36]. For the frequency sweep measurement, lying within quasi-LVE region, a constant strain of $\gamma = 0.1 \%$ was applied whilst angular frequency (ω) spanned the range of $0.01 - 100 \text{ (rad)s}^{-1}$. The viscoelastic moduli, storage modulus (G') and loss modulus (G''), were evaluated using amplitude sweep measurements as a function of strain amplitude (γ) and frequency

sweep measurements as a function of angular frequency ($\omega = 0.1-100$ (rad) s^{-1}). Complex viscosity (η^*), derived from the viscoelastic moduli, was, therefore, also followed as a function of increasing angular frequency. To define differences between the respective suspensions regarding their colloidal interactions, packing effects and friction between graphite nanoflake agglomerates and nanofibrils during the flow, log-log plot flow curves of the complex viscosity (η^*) were also fitted to a power law according to an equivalent of the Ostwald-de Waele empirical model [41]. For oscillatory measurements, using an effective shear rate determined as the root mean square value under oscillation, the effective dynamic viscosity beyond the quasi LVE region, can be expressed as shown in Eq. (2) [34],

$$\eta^* = k_c (\dot{\gamma}_{\text{rms}})^{n_c-1} = k_c \left(\frac{\sqrt{2}}{\pi} \omega \right)^{n_c-1} \quad (2)$$

where k_c and n_c are the flow consistency index and the power-law exponent, respectively, for the complex viscoelastic case: $n_c = n = 1$ indicates a Newtonian fluid, whereas $n < 1$ indicates a pseudo-plastic (shear thinning) behaviour.

2.5.3 Consecutive yield stress

Yield stress is perhaps the most important rheological property of complex suspensions, as it needs to be exceeded in order that they can flow, which is challenging to evaluate for such wall slip/solids depletion prone materials as NFC-containing suspensions, which display shear banding to minimise stress when sheared [38,46]. Therefore, both the static yield stress (τ_s^0), obtained from the quasi-LVE region conducted with plate-plate geometry, and the dynamic yield stress (τ_d^0), from flow curves conducted from vane in cup geometry are used. The dynamic yield stress (τ_d^0) is defined as the minimum stress required for maintaining the flow, while static yield stress (τ_s^0) is defined as the stress required for initiating flow, and the latter often has the higher value for MFC suspensions [34,47].

The Herschel-Bulkley equation describes the presence of a dynamic yield stress (τ_d^0) from the plot of the flow curves as shown in Eq. (3),

$$\tau_d = \tau_d^0 + k\dot{\gamma}^n \quad (3)$$

where the terms k and n are the consistency and flow index, respectively, as presented in Eq. (1), with, once again, the value of $n < 1$ describing a material exhibiting shear thinning, and $n = 1$ Newtonian behaviour [38,40].

2.6 Characterisation of materials and suspensions

2.6.1 Preparation of nanocellulose and graphite-MFC/HTC films

Samples for morphological characterization of HTC were prepared according to the procedure described by Buffiere *et al.* [29]. An aqueous HTC suspension of 15 w/w% was frozen by submersing in liquid nitrogen, and the samples were freeze-dried for 24 h. The final preparation stage consisted of grinding freeze dried samples using a mortar and pestle. For observation of morphology and internal structure of raw material MCC and MFC, and graphite nanoflakes in aqueous suspension, films were prepared by pouring the suspension onto Whatman filter paper in a porcelain Büchner funnel with 5 mm holes. A further filter paper was placed on top of the suspension and the whole placed under vacuum filtration. After filtration, films were loaded under two stainless steel plates to prevent shrinkage and dried at room temperature for 24 h followed by drying in an oven at 50 °C for a further 24 h [48].

2.6.2 Degree of polymerisation

Size-exclusion chromatography (SEC) was used to determine the degree of polymerisation (DP) of the cellulosic materials. The setup comprised of a Dionex Ultimate 3000 system equipped with four identical columns (PLgel Mixed-A, Agilent, USA) and a refractive index (RI) detector (Shodex RI-101, Showa Denko K.K., Japan). The samples were activated and dissolved in DMAc/LiCl₂ (9.0 g.dm⁻³) according to a solvent exchange-based method already described elsewhere [27]. The RI chromatograms were then calibrated against a series of eleven narrow pullulan standards with molecular weights ranging from 342 Da to 2 560 kDa from which the weight-average DP was extracted [28,39].

2.6.3 Morphological properties of graphite-nanocellulose films

Scanning electron micrographs (SEM) were obtained using a Sigma VP setup (Zeiss, Germany) to characterise the morphology of the MCC, MFC and HTC [23,29]. One drop of 0.1 w/w% suspensions of MCC/MFC were placed on a high-purity mica surface and dried on a hot plate at 60 °C for 10 min. The sample was further outgassed and dried under vacuum and sputtered using an Emitech K100X glow discharge apparatus (Quorum Technologies, Lewes, UK) equipped with an Au/Pd electrode with a current of 30 mA for 60 s, corresponding to a sputtered layer of around 7 nm. The samples of HTC were prepared by freeze-drying, followed by sputtering with a ~4 nm platinum film. To visualise the structure of the MCC, MFC and graphite nanoflake-MFC/HTC composites micrographs were recorded using a secondary electron detector, an accelerating voltage of 1.0 kV, at a working distance of 5 mm. No further processing was applied to the micrographs other than contrast and brightness correction.

2.6.4 Microstructural characterisation of nanocellulose

X-ray diffraction (XRD) of both HTC powders, described in Buffiere *et al.* [27,30], and MCC/MFC nanocellulose films, described in Vanhatalo *et al.* [23], was carried out with a Bruker D8 Advance diffractometer (Bruker, Santa Barbara, CA, USA). The crystallite size for MCC and MFC was determined by applying the Scherrer equation using the {020}, {110} and {1-10} lattice planes for HTC [27]. The peak width of HTC samples was measured with DIFFRACEVA software according to the Segal equation, applying peak deconvolution, and when possible in addition with the XRD peak height method according to earlier described method [30,49].

2.6.5 Particle and agglomerate size in suspension

The particle size distributions of the water medium-processed and post-process mixed agglomerate structures were measured with a Mastersizer (Malvern Instruments, Malvern, UK) to illustrate the role of MFC and HTC particle size on graphite dispersion in the process [24,34]. Prior to measuring, the samples were diluted with de-ionised water to a solid content of 0.01 w/w%. The light scattering volume equivalent median diameter ($d_{sv}(50)$) is also reported as an average of at least five separate measurements. In the case where the density of a material is constant throughout its size distribution, the volume and weight determined size distribution are identical.

2.6.6 Morphological properties of nanocellulose particles

Atomic-force microscopy (AFM) apparatus (Dimension 3000, Bruker, Santa Barbara, CA, USA) was used to estimate the dimensions of MCC and MFC nanocellulose, described in detail in Vanhatalo *et al.* [23] and Buffiere *et al.* [30]. Dynamic light scattering (DLS) volume equivalent median diameter ($d_{sv}(50)$) was used for the measuring of particle size of MCC (Merck) raw material.

2.6.7 Contact angle

The surface free energy of the materials was assessed using liquid-surface contact angle between a film prepared with vacuum filtration and liquids [48,49]. Four liquids of known surface tension were

used in static droplet mode using a CAM 200 (KSV Instruments, Helsinki, Finland) goniometer, namely deionised water, diiodomethane, formamide and ethylene glycol. A drop of liquid up to 6.2 μL from a microsyringe was automatically dispensed onto the surface of the film. When the drop touched the film surface, its image was recorded with a CAM 2008 software. The average droplet receding contact angle, θ_r , as a function of time of each of the four pure liquid probes was measured from the recorded images, and the wetting condition calculated using the Young-Laplace equation. An average of five separate analyses on the same film was used, and the resulting surface energy components (dispersive Lifshitz-van der Waals (σ^{LW}) and polar acid-base (σ^{AB}) and total solid surface energy (σ^{tot}) evaluated.

2.6.8 Electrical conductivity

Electrical conductivity was measured by the four-cell, or four band, technique using a digital conductivity meter CG 855 instrument (Yumpu, Diepoldsau, Switzerland). The conductivity cell consists of 4 bands along the measuring column. An AC voltage is applied across the two outermost bands (correcting bands), which causes a current flow through the measuring cell [15,33]. Five specimens were tested, and the average value was calculated.

3. RESULTS AND DISCUSSION

The first sub-section discusses the influence of structure and particle morphology of the MFC and HTC particles on the structural properties of the corresponding graphite-nanocellulose suspensions [17,41]. The second sub-section evaluates rheological results obtained from viscoelastic and steady state shear measurements. The third sub-section focuses on the electrical conductivity and surface energy of graphite-HTC suspensions [25,26,50].

3.1 Particle morphology and physical properties: influence on the dispersion of MFC and HTC

The process methods for MFC and HTC are shown schematically in Fig. 1. In addition a summary of morphological and surface energy data for MFC and HTC is presented in Table 2 [22,23]. The SEM micrographs in Fig. 1 show that the two types of cellulose particles have nanoscale features and relatively high aspect ratio [23,30]. However, the HTC material consists of homogeneous flat ribbon-like particles, compared with the more fibrillar and interconnected structure of MFC [30]. This is in line with previous findings, which identified that the supercritical water treatment of MCC towards HTC leads to the formation of regenerated cellulose II particles, with a specific ribbon-like crystal morphology [29,30].

As presented in Table 2, the MCC (Avicel) used for production of MFC had a DP of 274 [23]. Mechanical process of production of MFC from MCC consisted in creating high shear within a chamber to create friction, which triggers the physical deconstruction of the particles but without significantly altering the cellulose crystallites nor the DP of the cellulose [1,21]. As a result, the DP of 243 for MFC remained close to that of MCC. In contrast to this, with an average DP of 50, HTC particles had in contrast significantly lower molecular weight [29,30].

The difference between the two materials was not only in morphology and structure, but also in surface properties. This was revealed by contact angle measurements and surface free energy values for MFC and HTC, as shown in Figure 1. The polar and acid-base components of the surface free energy were both higher in case of HTC, which led to a total surface free energy approximately 10 $\text{mJ}\cdot\text{m}^{-2}$ higher than that of MCC and MFC. This indicates a significantly stronger wettability for HTC than for MFC [34,48]. The increase in surface free energy can be explained by the specific processing method, in which cellulose chains rearrange themselves upon precipitation after supercritical water treatment into the more thermodynamically stable cellulose II conformation rather than the starting cellulose I β allomorph, the crystal structure of native cellulose found in most plants and most cellulosic materials. This rearrangement has been shown to enhance the amphiphilic behaviour of cellulosic fibres [51].

Together with the ribbon-like morphology, this structural difference can be expected to contribute to better dispersion and penetration within hydrophobic agglomerates of graphite nanoflakes, as already witnessed in Pickering emulsions [30].

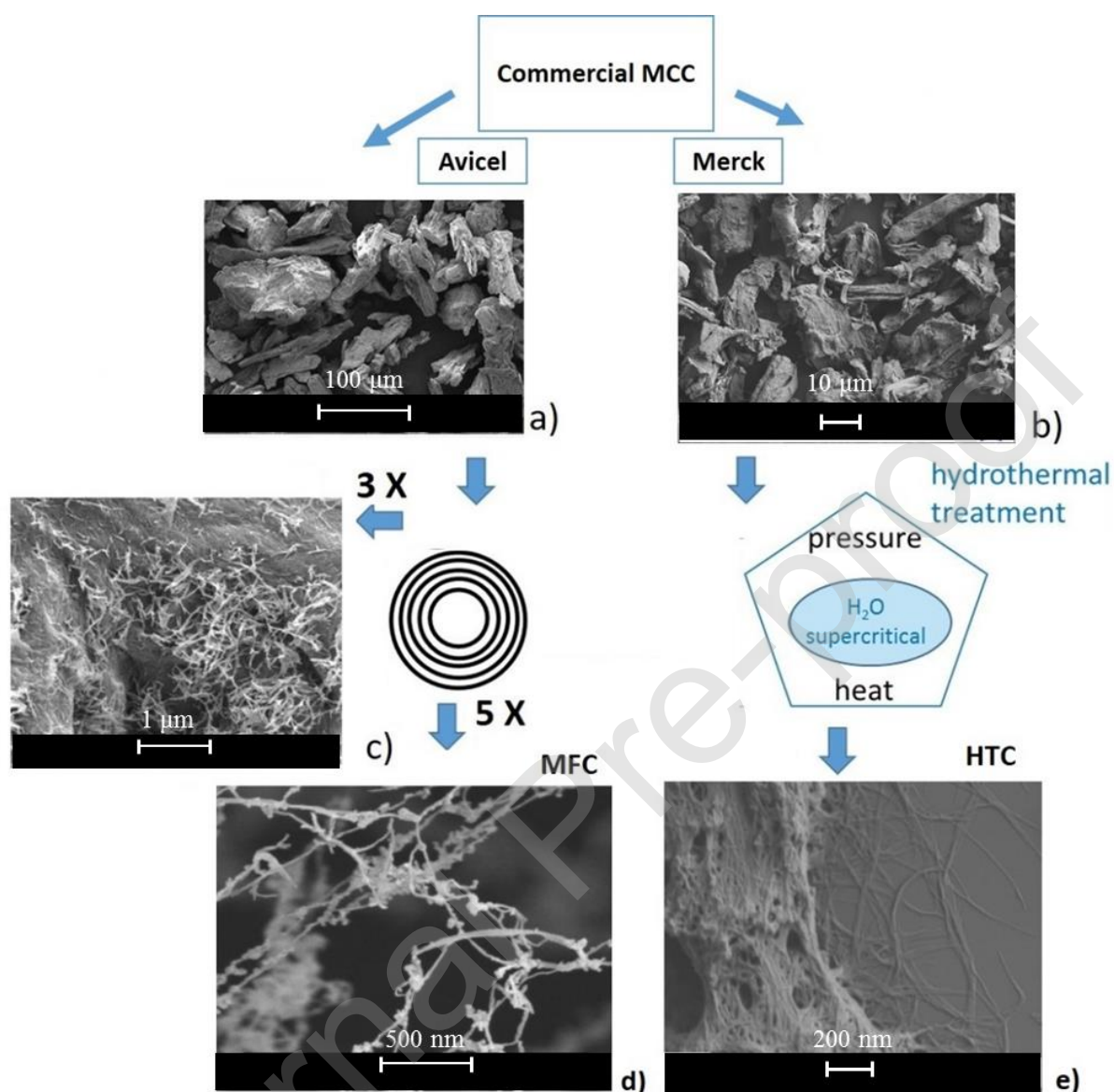


Fig. 1 Schematic representation of production of MFC and HTC suspensions from MCC feed materials with SEM micrographs of the corresponding materials: a) Avicel raw MCC used for microfluidisation, b) Merck MCC raw material used for hydrothermal treatment, c) MFC obtained in a fluidiser at 20 MPa, (from a)) after 3 fluidising cycles, d) MFC obtained in a fluidiser and e) production of HTC in supercritical water reactor.

The supercritical water treatment method influenced the rearrangement of cellulose chains in the nanocellulose and crystallite size increased from raw material MCC (Merck) 7 nm to 12 nm (± 1 nm) for HTC, as reported previously [27]. As expected, microfluidisation by contrast did not affect crystallinity or cellulose structure during the multiple passes through the fluidiser, i.e. virtually unchanged from MCC (Avicel) 4 nm to 3.8 nm (± 1 nm) for MFC, as observed previously for same procedure [22,23].

The supercritical water treatment and high shear homogenisation, Table 2, both yielded nanoscale cellulose particles with radically different morphologies and colloidal properties of nanocellulose.

Table 2. Properties of MFC and HTC products used in this study.

Sample	Approximate particle length (HTC), L / nm	Approximate particle width (HTC), W / nm	Approximate particle thickness (AFM), T / nm	Degree of polymerisation, DP	total free surface energy σ^{tot} $ / \text{mJ.m}^{-2}$
MCC (Merck)	N.A.	N.A.	22 000	340	33.8
MCC (Avicel)	N.A.	N.A.	58 000	274	36.3
MFC	500	10	10	243	37.4
HTC	800	40	5	50	47.7

Therefore, suspensions with the same volume but different total consistency were formed, as displayed in Table 1, also shown schematically in Fig. 2. Although this method does not allow calculating a dispersant demand due to changing solids content induced by addition of dispersant also in aqueous suspension, the results are nonetheless suitable to compare the efficiency of each dispersing system with each other.

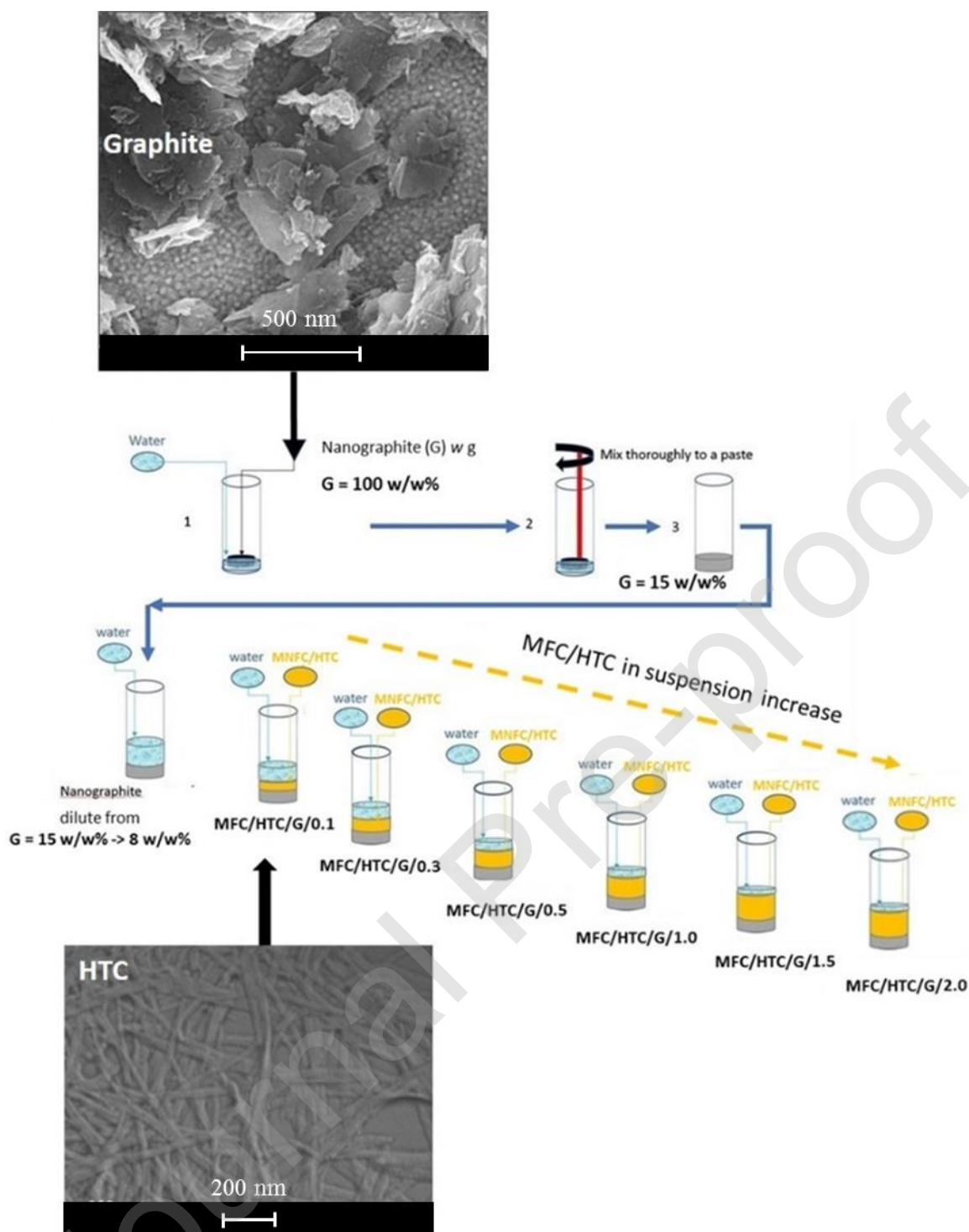


Fig. 2 Schematic representation of preparation of MFC/HTC-graphite suspensions, according to standard SCAN-P 55:88, SEM image of graphite nanoflakes [by kind permission of Asbury Carbons, 156 Asbury-West Portal Road, Asbury, NJ 08802, USA, www.asbury.com], and SEM micrograph showing the film formed from particles comprising the HTC material.

SEM images obtained from samples in which HTC was used as dispersing agent of graphite nanoflake suspension are shown in Fig. 3. The micrographs reveal that, upon addition of HTC particles, initially highly flocculated graphite nanoflakes became dispersed. Undispersed, graphite nanoflakes showed a sample surface that was either fully covered or had large cracks, which were completely free of particles. This indicates strong agglomeration, and film shrinkage upon drying. Upon addition of HTC

as dispersing agent, the sample surface changed to a network of finer cracks, and onwards towards complete disappearance of cracks at 2 w/w% of HTC in the graphite nanoflake suspension, resulting in a smooth coverage by the sample layer, G/HTC/2.0.

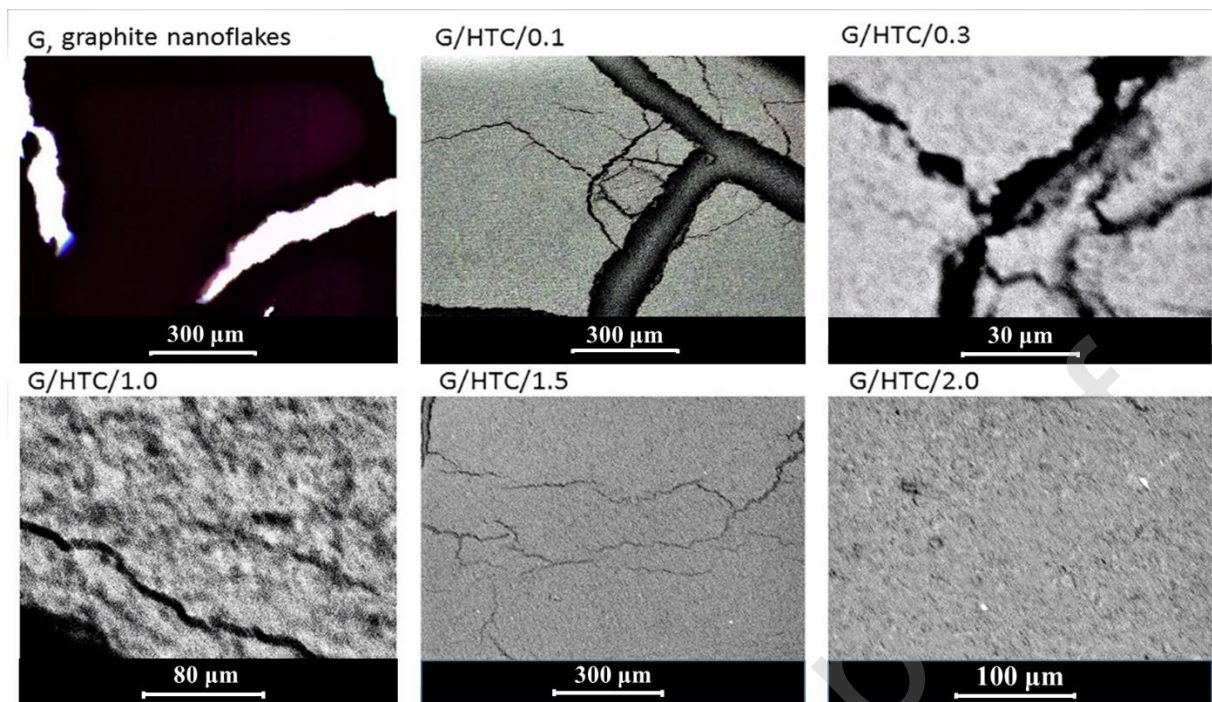


Fig. 3 SEM images revealing the dispersing effect of 0.1 w/w%, 0.5 w/w%, 1.0 w/w% and 2.0 w/w%, respectively. These images display the transition from parts of undispersed graphite nanoflakes showing large cracks through to good dispersion displaying a much finer crack network, and finally the surface fully continuous when there is sufficient HTC present to form a coherent film.

As the nature of the treatment changes the morphology of the cellulose particles, this in turn influences their interaction and network-forming ability, in this case without any chemical modification of the particles themselves [30,41]. Films made of pure HTC exhibited significantly denser structures, resulting partly from greater particle-particle surface interactions linked to the ribbon-like morphology favouring closer interparticle contact points. The SEM images from Fig. 4 also indicates that the average agglomerate size of graphite nanoflake suspensions decreases with addition of both MFC and HTC.

When films were obtained from samples from Table 1, their micrographs further reveal that cellulose nanofibrils, both MFC and HTC have a dispersing effect on graphite nanoflakes and their agglomerates, as seen in Fig. 4. When dispersed with MFC, these films viewed in cross-section have a hairy-like appearance and display a greater tendency to cracking than the HTC containing films. This is likely related to the establishment of a shrinkage density gradient within the structure of flocculated graphite nanoflakes and entangled MFC fibrils - the more hydrophilic nature of the MFC retaining more water and hence greater shrinkage on drying, Fig. 4a). In contrast, upon dispersing with HTC, graphite nanoflake-containing layers become oriented horizontally, due to the interfacial interaction between higher surface free energy of HTC particles, with less retained water, as seen in Fig. 4b). As a result, films made from graphite nanoflakes dispersed with HTC particles formed three-dimensional networks, significantly denser than that of the entangled MFC fibrils.

The amphiphilicity of HTC is well exemplified by the comparison of contact angle using deionised water: the average contact angle was 43° for HTC and 72° for MFC, and the affinity of HTC for the hydrophobic graphite nanoflakes is thus complementarily displayed in respect to its dispersibility [15,17]. Therefore, the fact that the contact angle is lower for the HTC, but also the good dispersibility

of hydrophobic graphite nanoflakes, mean that the complementary hydrophobic part is nonetheless able to be strongly manifest when attaching to the graphite surface.

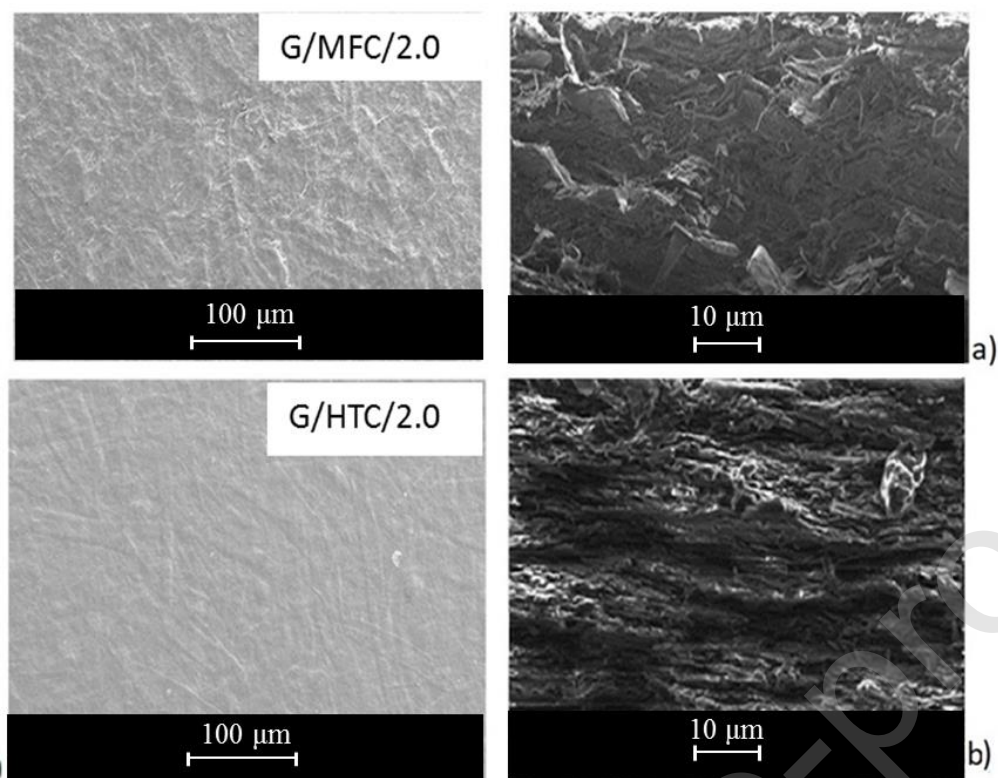


Fig. 4 SEM images of films; surface (left) and cross-section (right) of a) 2 w/w% MFC and b) 2.0 w/w% HTC dispersions of graphite nanoflakes with MFC and HTC particles, respectively. Note the clear packing differences, with visible hair-like structures seen in the MFC-containing layer.

The effect of nanofibrils is to disperse graphite by coupling with agglomerates under shear, transmitting the torque generated across the shear planes and therefore prising open agglomerates, giving a closer packed and more uniformly oriented structure for HTC than for MFC dispersing particles. The SEM visual assessment, Fig. 4, is supported by the static laser light scattering particle size data of the graphite nanoflake-nanocellulose suspensions, indicating changes in agglomerate size as shown in Fig. 5 and Table 3. This clearly reveals a decrease of graphite flake agglomerate size and that the dispersing effect of HTC is significantly higher than that of MFC.

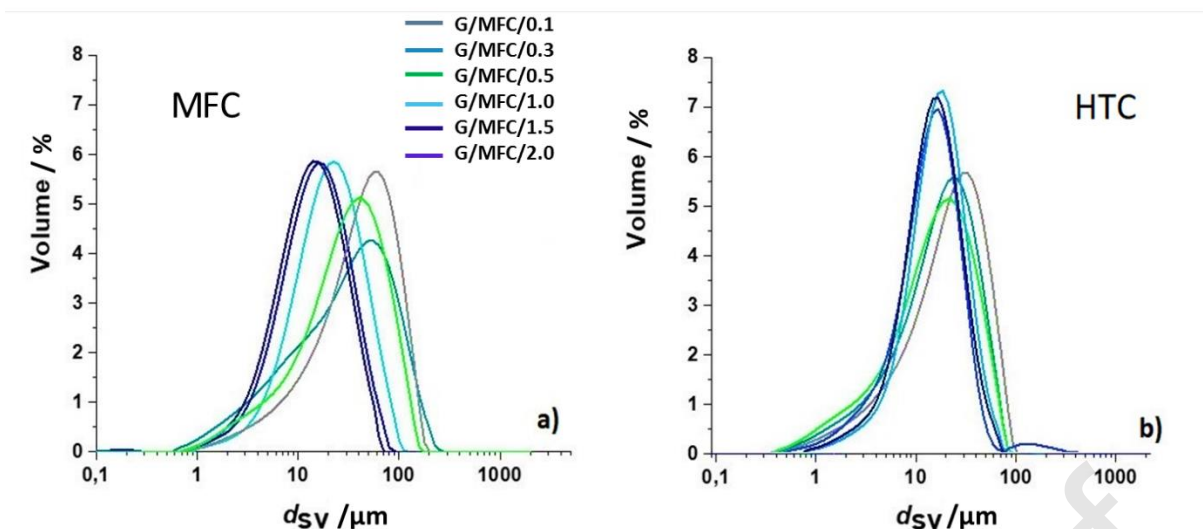


Fig. 5 Examples of the scattering volume equivalent agglomerate particle size distributions measured using static light scattering of graphite-nanocellulose suspensions: a) mixing with MFC, b) mixing with HTC.

The volume median agglomerate size, Fig. 5, appears highly dependent on the type of micro/nanocellulose used for dispersing, primarily in respect to the surface energy and morphology of the cellulose component. Although the finer agglomerate size is observed for graphite nanoflakes dispersed with HTC, the agglomerate size of graphite suspensions decreases upon additions of 1 w/w% and 2 w/w% for both MFC and HTC, with more pronounced effect in case of HTC dispersant. This supports the hypothesis of intrinsic structure controlling effect of nanocellulose particles, correlating with the results visualised in the SEM images.

Table 3. Volume median agglomerate size, $d_{sv}(50)$, as measured by static light scattering comparing water medium dispersing when mixing graphite nanoflakes with MFC and HTC, respectively, with constant suspension volume. MCC is also added for comparison, showing that the cellulose particles used in dispersing, derived from the MCC, have a smaller equivalent spherical size than the graphite nanoflakes.

Sample	Scattering volume equivalent median diameter, $d_{sv}(50)$ / μm
G/MFC/0.1	220.56
G/MFC/0.3	135.86
G/MFC/0.5	119.49
G/MFC/1.0	79.49
G/MFC/1.5	64.51
G/MFC/2.0	59.64
G/HTC/0.1	120.00
G/HTC/0.3	98.16

G/HTC/0.5	61.36
G/HTC/1.0	53.85
G/HTC/1.5	38.89
G/HTC/2.0	25.81
MCC	11.23

3.2 Rheology

This section evaluates the rheometric analysis of the dispersing effect of MFC and HTC, respectively, on graphite nanoflakes in aqueous suspension. Increased stress during shearing induces break-up of graphite clusters and enables nanosized cellulose particles to enter into graphite agglomerates and add to dispersion within the suspension matrix [52]. Apart from the complex rheological behaviour expected from graphite nanoflakes as they tend to agglomerate [13,34,36], the particle-particle aggregation structure at low strain reveals trend in respect to the dispersing effect of the two different types of nanocellulose, MFC and HTC. Amplitude sweep measurements, shown in Fig. 6a) and b), reveal different levels of flocculation for graphite nanoflake suspensions where MFC was dispersing agent, Fig. 6a), from those where HTC-dispersant was acted to disperse graphite agglomerates [33,34]. Reduced storage modulus (G'/G'_0) and reduced loss modulus (G''/G''_0) display the effect of the suspension flocculation and phase separation at higher strain observed as an increase in G''/G''_0 once the critical strain (γ_c) is exceeded due to aggregation, while G'/G'_0 decreases [41,46,47].

This difference is manifested only for samples with a lower load of HTC (G/HTC/0.1, G/HTC/0.2), Fig. 6b). In contrast, the larger scale loose floc structure is associated with longer and more networked MFC particles, which decreases upon addition of more such fibrils. In contrast, in the case of shorter and more crystalline HTC particles a dispersing effect which is observable at much smaller doses [50,53].

The strain levels are chosen to reflect the two-stage structure regime, i.e. initial presence of agglomeration at $\gamma = 0.01$ %, and latterly upon the cross-over of the quasi-linear elastic region (LVE), at $\gamma = 1.12$ %, before reaching a critical strain γ_c , at which the elastic moduli drastically decrease.

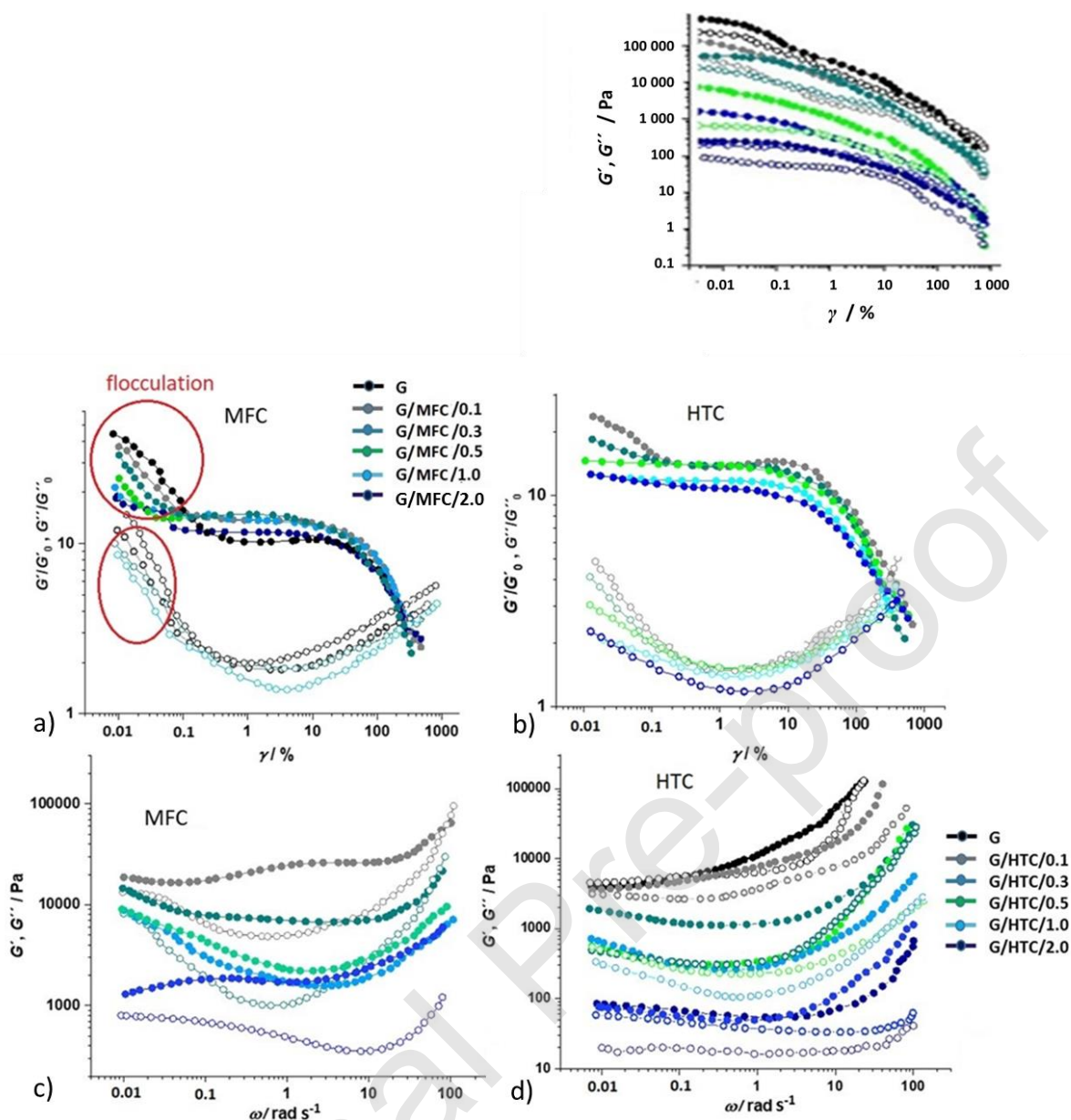


Fig. 6 Viscoelastic moduli G' (solid symbols) and G'' (open symbols) obtained from amplitude sweep tests: a) and b) reduced values of storage modulus G'/G'_0 and loss modulus G''/G''_0 for MFC and HTC dispersed graphite nanoflakes, respectively; the insert in b) viscoelastic moduli G' (solid symbols) and G'' (open symbols) behaviour as a function of strain. These are compared with the G' and G'' c) and d) obtained from frequency sweep for MFC and HTC dispersed graphite nanoflake suspensions, respectively.

The values in Table 4 also clearly indicate that suspected increased coupling between MFC and graphite nanoflake particles when the two are co-exfoliated, via co-processing, is supported by comparatively higher structural strength and viscoelasticity than for simpler aggregates of HTC-dispersed graphite nanoflakes, i.e. $\{G', G'' (G/MFC)\} > \{G', G'' (G/HTC)\}$, respectively.

The elastic moduli (G' and G'') of all the graphite nanoflake-MFC composite suspensions show similar response to increasing angular frequency (ω) under oscillation, Fig. 6c) and d), displaying initially weak structure breakdown, as was seen under low shear microscopy sample preparation, Fig. 4, followed by high frequency vibration-induced elastic behaviour [34,54]. This observation clearly indicates that the stronger aggregation structure of graphite nanoflake suspension in the MFC medium becomes

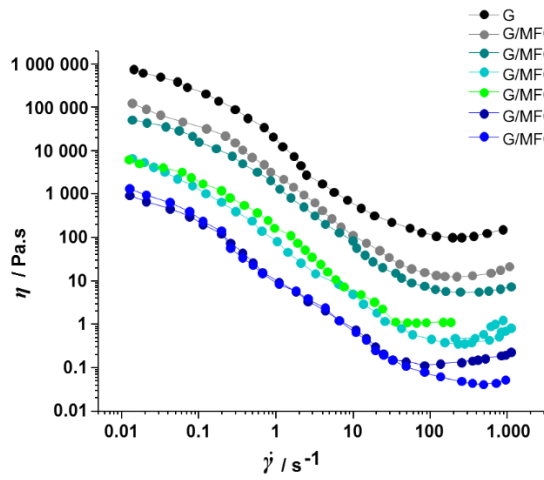
ever more rigid under vibration, following a hardening response. Again, the better dispersing effect of HTC-containing samples due to the weaker initial static structure can be observed with lower values of both elastic G'/G'_0 and loss G''/G''_0 moduli at low strain and lower dependence of angular frequency, Fig. 6b) and d), respectively. For both MFC and HTC at lower fibril amounts, the vibration, Fig. 6c) and d), induces elastic hardening, seen as a cross-over from the lowest modulus (G' and G'') values at low angular frequencies (ω) to the highest or close to highest at high frequency [42,55,56]. This effect is reduced at higher HTC levels, which is higher dose of dispersant in suspension.

Table 4. Values of elastic (G') and loss (G'') moduli at two different values of strain ($\gamma = 0.01\%$ and 1.12%), capturing the two-stage structure breakdown of loose flocs followed by stronger aggregates.

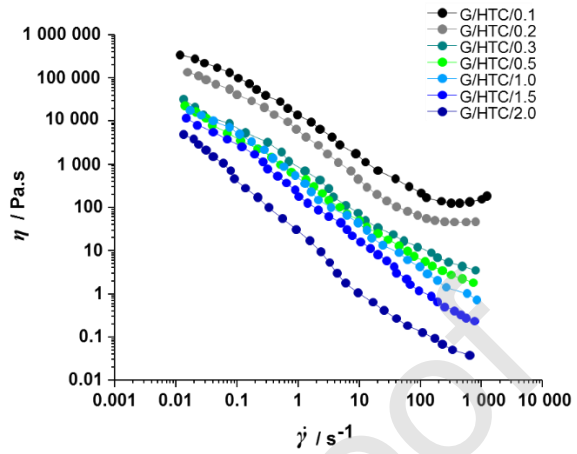
Addition of MFC/HTC graphite nanoflakes, G	Elastic modulus G'			
	/ Pa			
	$G'_{\gamma = 0.01\%}$		$G'_{\gamma = 1.12\%}$	
	G/HTC	G/MFC	G/HTC	G/MFC
G/0.1	1 203.23	379.43	198.34	243.23
G/0.3	185.23	221.23	138.94	154.32
G/0.5	124.78	199.12	109.91	88.52
G/1.0	89.56	102.23	83.25	99.13
G/1.5	88.09	99.12	76.13	89.52
G/2.0	37.76	59.34	53.52	62.75
	Loss modulus G''			
	/ Pa			
	$G''_{\gamma = 0.01\%}$		$G''_{\gamma = 1.12\%}$	
	G/HTC	G/MFC	G/HTC	G/MFC
G/0.1	131.96	143.12	121.77	129.67
G/0.3	125.43	131.41	95.88	81.52
G/0.5	88.28	95.43	82.74	78.49
G/1.0	56.76	79.56	10.86	16.41
G/1.5	34.96	42.36	9.14	13.57
G/2.0	21.78	33.23	8.23	11.21

The shear thinning behaviour of graphite nanoflake-nanocellulose suspensions within the viscoelastic region under oscillation was traced using the complex viscosity (η^*) response to increased angular frequency (ω) under constant strain, as presented in Fig. 7a) and b) [43,54]. Shear thinning behaviour at low and intermediate angular frequencies with MFC as dispersant, evolves towards dilatant behaviour at higher frequencies, which is less pronounced when HTC particles are used for the dispersion of graphite nanoflakes, while it remains present for all given additions of MFC medium. This effect is typical for rheological behaviour of graphite suspensions due to hydrophobic agglomeration,

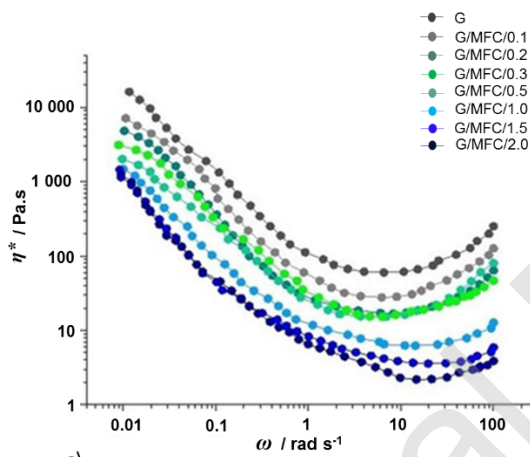
but when HTC is used as dispersing agent, this high shear rate induced dilatancy is present only for the suspensions in which graphite nanoflakes dominate, decreases already at 0.3 w/w% addition [36,44].



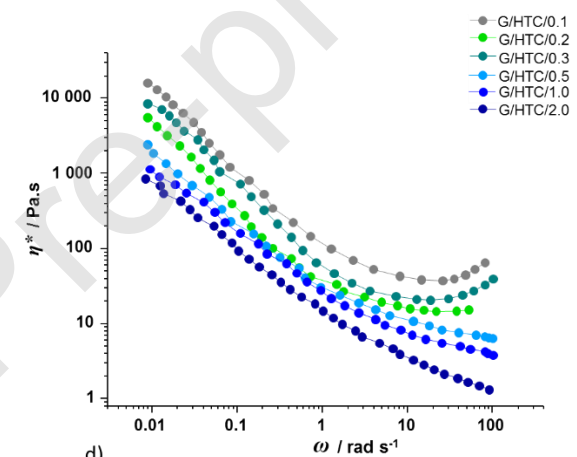
a)



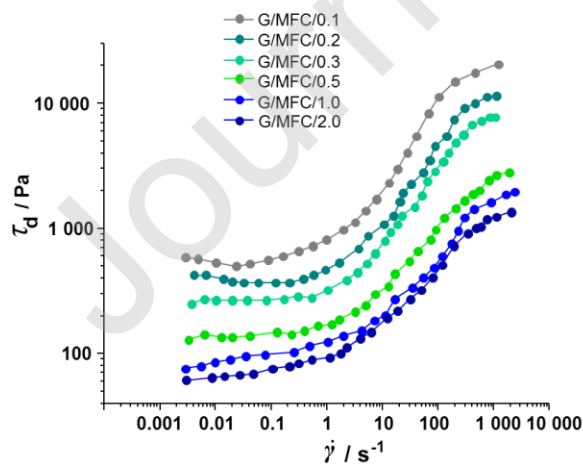
b)



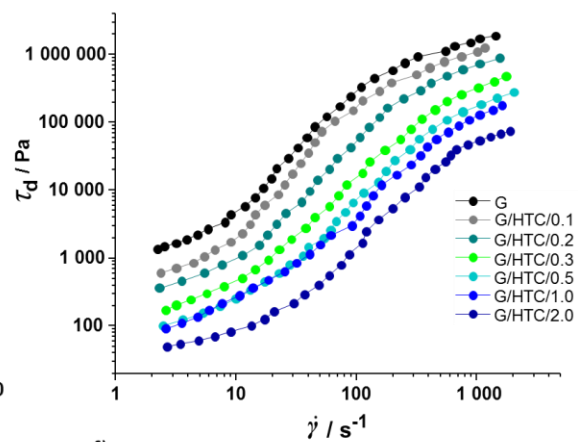
c)



d)



e)



f)

Fig. 7 a) and b) dynamic (η), c) and d) complex viscosity (η^*) comparison of initial response to increase of shear rate $\dot{\gamma} = 0.001 - 1\,000\text{ s}^{-1}$ and angular frequency $\omega = 0.01-100\text{ (rad)s}^{-1}$, respectively, for the addition of MFC and HTC to the graphite nanoflake dispersion, following the Ostwald-de Waele viscosity and complex viscosity thinning analogue described by the parameters k and n , and k_c and n_c , respectively, showing the region of high frequency induced dilatancy; e) and f) rheograms of dynamic stress (τ_d) of MFC- and HTC-dispersed graphite nanoflake suspensions.

Due to the thixotropic behaviour seen in the steady state flow curves, Fig. 8, fitting according to the Ostwald-de Waele power law, Eq. (1), for dynamic viscosity (η), Eq. (2), can be used only by defining segments along the rheograms according to three shear rate intervals [34,38]. The first is due to initial agglomeration at low angular frequency and low shear rate, the second related to thinning by breakdown of the structure and, finally, the third showing hardening at higher deformation rates. The low angular frequency and low shear region provides confirmation of the initially sheared graphite flake flocs, while at medium shear the breakdown of stronger agglomerates and transition minimum of the structured state occurs, and the short region of quasi-steady state is reached [44,46]. The rheograms were, therefore, divided logarithmically into three interval regions, ($i = 1$) ultralow shear $\dot{\gamma} = 0.01 - 0.1\text{ s}^{-1}$, ($i = 2$) intermediate region $\dot{\gamma} = 0.1 - 100\text{ s}^{-1}$, and ($i = 3$) a high shear region $\dot{\gamma} = 100 - 1\,000\text{ s}^{-1}$.

By studying the power law coefficients k and n , for dynamic viscosity (η), fitting the rheograms to a power law in the intermediate shear rate domain ($i = 3$), it is possible to study the dispersing effect upon progressive increase of MFC and HTC in the suspensions. By studying this intermediate shear region in detail, and thereby avoiding both the area of floc and agglomerate structures at very low shear rates and the dilatant/shear thickening region at higher shear rates, it is possible to achieve a direct measure of particulate dispersibility. After fitting the intermediate intervals, it is possible, therefore, to define dispersing effect, as a decrease in flocculation and agglomeration (decrease of k_i) and shear thinning (increase of n_i) in Fig. 8 [34,38,46].

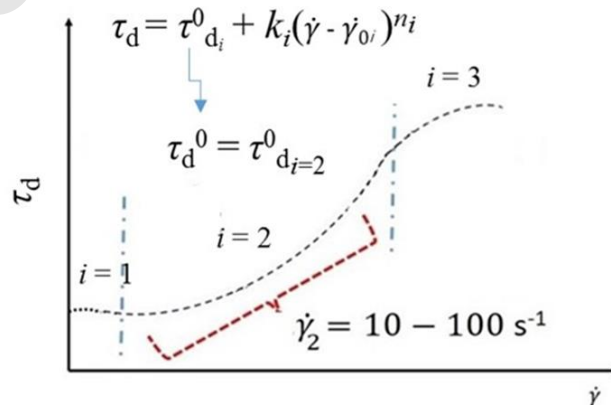
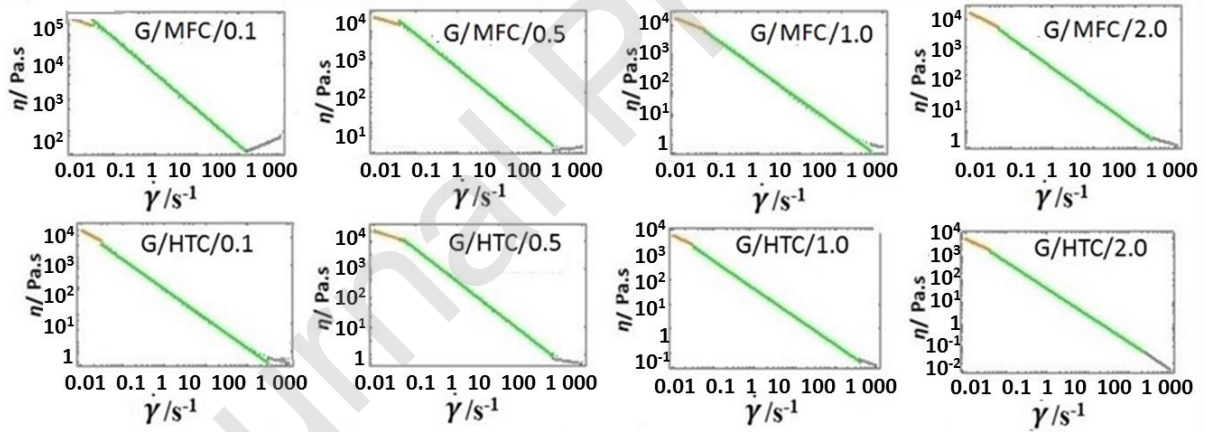


Fig. 8 The three interval regions of exponential change, showing the so-called “fourth characteristic” behaviour of stress growth fitted in region $i = 2$ using the Herschel-Bulkley expression.

3.3 Electrical conductivity and surface energy

The electrical conductivity of the HTC dispersed graphite nanoflakes films and their contact angle values for water and diiodomethane are shown in Table 5.

Table 5. Contact angles for water and diiodomethane on the HTC dispersed films, and their related electrical conductivity.

Sample	Water Contact angle / °	Diiodomethane Contact angle / °	Electrical Conductivity / S.m ⁻¹
G/HTC/0.1	22.4 ± 1	44.2 ± 2	1.80 × 10 ³
G/HTC/0.3	20.8 ± 1	43.5 ± 2	1.40 × 10 ³
G/HTC/0.5	20.0 ± 2	39.7 ± 2	1.00 × 10 ³
G/HTC/1.0	19.4 ± 1	37.8 ± 2	0.95 × 10 ³
G/HTC/1.5	19.2 ± 1	34.1 ± 3	0.84 × 10 ³
G/HTC/2.0	19.1 ± 1	37.6 ± 3	0.77 × 10 ³

The difference between the two materials, MFC and HTC, in morphology and rheology manifest themselves in different surface properties of nanoflake films (Tables 5 and 6). The electrical conductivity naturally falls as the proportion of nanocellulose increases, being related to the loss of graphite nanoflake-nanoflake contact. The difference in rate of decrease rightly illustrates the added value of the HTC nanocellulose versus the fibrillar MFC, since less is required to achieve good dispersion, and thus the conductivity result at optimal dispersion is enhanced [18,19].

For completeness, the surface tension parameters of the liquids, taken from literature, are shown in Table 6. The surface energy of the composite films changes only very little in respect to the HTC nanocellulose component amount, Table 6. This reflects the compatible surface nature of the HTC in respect to the graphite nanoflakes, in that lower doses of HTC dominate the composite consistent with the improved dispersion of the nanoflakes amongst the HTC fibrils [55,56].

Table 6. Literature free surface tension parameters for the probe liquids and calculated surface free energy of the films.

Liquid	Free surface tension / mN.m ⁻¹
	σ^{tot}
Water	72.8
Formamide	58.0
Diiodomethane	50.8
Ethylene glycol	48.0
Films	Surface energy / mJ.m ⁻²
G/HTC/0.1	64.9
G/HTC/0.3	65.9
G/HTC/0.5	64.9

G/HTC/1.0	65.3
G/HTC/1.5	65.3
G/HTC/2.0	65.3

From Table 7, it is seen that the stronger dispersing power of HTC particles enable graphite nanoflakes to align with the flow, similar to that observed in the SEM images, Fig. 4b). The multistep approach with the concatenated Herschel-Bulkley models, described in our previous research on co-exfoliation of graphite flakes and nanocellulose enables rheological parameterisation of dispersion in nanocellulose-graphite composites [34].

By observing the difference in magnitude of dynamic yield stress ($\tau_{d_2}^0$) from steady state measurements, and static yield stress ($\tau_{s_2}^0$) from amplitude sweep measurements, in the intermediate interval the dispersing effect of MFC and HTC can be parameterised to quantify the decrease in flocculation and agglomeration, in favour of more crystalline and smaller HTC [30,50]. Both static, τ_s^0 , and dynamic, τ_d^0 , stress as a function of strain display information in respect to describing the different dispersing of highly aggregated and flocculated graphite nanoflake particles, plotted in Figs. 7c)-d). Table 7 also provides insight into the dispersing effect differences between MFC and HTC on graphite nanoflakes from each i domain concatenation point [41,43,44]. Fitted curves of the complex viscosity (η_i^*) response over the intermediate region ($i = 2$) to increasing angular frequency ($\omega = 1-10 \text{ rad.s}^{-1}$), provide the dispersing effect parameterisation with values of flow $k_{c(i=2)}$ and shear thinning coefficient $n_{c(i=2)}$.

Table 7. Stress and viscosity curve parameterisation obtained by using the power law models, Eqs. (1) and (2), and the method from Fig. 8.

$i = 2$	Fitted intermediate region shear rate response						
	G	G/MFC/0.1	G/MFC/0.3	G/MFC/0.5	G/MFC/1.0	G/MFC/1.5	G/MFC/2.0
$\tau_{s_i}^0$ (Pa)/MFC	3 117.30	2 989.88	2 554.99	1 739.89	1 088.37	923.43	695.79
$\tau_{d_i}^0$ (Pa)/MFC	29 234.56	2 647.17	2351.35	1 623.17	978.36	915.04	632.24
n_i	0.26	0.22	0.19	0.16	0.13	0.11	0.09
k_i	26.45	19.67	17.34	15.76	13.12	9.34	7.56
	Fitted intermediate region frequency response						
	G	G/HTC/0.1	G/HTC/0.3	G/HTC/0.5	G/HTC/1.0	G/HTC/1.5	G/HTC/2.0
$\tau_{s_i}^0$ (Pa)/HTC	3 126.50	2 456.25	2 244.51	13265.27	885.45	674.173	492.51
$\tau_{d_i}^0$ (Pa)/HTC	26 528.45	2 398.32	235108.45	1 291.77	834.26	621.36	438.41
n_{c_i}	0.38	0.33	0.27	0.19	0.17	0.14	0.11
k_{c_i}	36.46	30.45	27.31	21.15	16.43	12.34	9.83

4. CONCLUSIONS

With microcrystalline cellulose (MCC) as starting material to yield MFC mechanically, and hydrothermal cellulose (HTC) via supercritical water treatment, this work reports the improved dispersing effect of HTC compared to the more traditional MFC for graphite nanoflakes.

While the processing of HTC under supercritical water conditions involves high temperature, and, thus, energy input, as well as high-pressure within a reactor system, the reaction transforming MCC into HTC is extremely fast, with no environmentally damaging chemicals employed for such a technically advanced product. Rheological parameterisation of the stress-shear rate response was used to characterise the dispersion within the complex nanographite/nanocellulose suspensions, and revealed significantly better uniformity of graphite nanoflake dispersion with HTC as dispersant compared with MFC. The improved suspension dispersion was subsequently reflected by the morphology of nanocellulose-graphite films formed from the dispersions as well as their conductivity and wettability.

The improved aqueous dispersibility of graphite nanoflakes with HTC has high industrial potential, not only for realising the advanced functionality of such nanomaterials, but also in respect to foreseen environmental benefits arising from heat recovery systems in HTC reactors. The greater dispersing efficiency of HTC necessarily also allows less cellulose particles to be needed as dispersant, compared with traditional mechanically produced MFC, which can contribute to further improvement in electrical conductivity of graphite-biomaterial composites.

The HTC material has properties similar to that of other nanocelluloses but is favourable in applications where a narrow size distribution of dispersant particles is needed, and where there an additional requirement for biodegradability or biocompatibility is present. This can create opportunities for use in numerous fields of endeavour where graphite nanoparticles are needed, for example, to improve the mechanical and/or electrical properties of composites, or to enable subsequent mechanical co-exfoliation of graphite towards few-layer graphene.

CRedit roles

Katarina Dimic-Misic; rheology , complex Suspension , data analysis of complex suspensions and films

Jean Buffiere ; preparation of HTC, experimental analysis of HTC, rheology; SEM; writing of manuscript

Monireh Imani; preparation of HTC-Graphite films, conductivity measurements and contact angle; data analysis, writing of manuscript

Kaarlo Nieminen; matlab processing of rheological data

Herbert Sixta; experimental set- up design of research in relation to HTC-graphite ; supervision

Patrick Gane; experimental set- up design of research in relation to HTC-graphite and nanocellulose - graphite suspensions; manuscript writing

Declaration of interests

The authors declare that they have no known competing financial interests or personal relationships that could have appeared to influence the work reported in this paper.

References

- [1] Y. Li, H. Zhu, F. Shen, J. Wan, S. Lacey, Z. Fang, H. Dai, L. Hu, Nanocellulose as green dispersant for two-dimensional energy materials, *Nano Energy*. 13 (2015) 346–354. <https://doi.org/https://doi.org/10.1016/j.nanoen.2015.02.015>.
- [2] T. Zimmermann, E. Pöhler, T. Geiger, Cellulose Fibrils for Polymer Reinforcement, *Adv. Eng. Mater.* 6 (2004) 754–761. <https://doi.org/10.1002/adem.200400097>.
- [3] V.B. Mohan, K. Lau, D. Hui, D. Bhattacharyya, V. Balaji Mohan, K. Lau, D. Hui, D. Bhattacharyya, Graphene-based materials and their composites : A review on production, applications and product limitations, *Compos. Part B*. 142 (2018) 200–220. <https://doi.org/10.1016/j.compositesb.2018.01.013>.
- [4] K. Hu, D.D. Kulkarni, I. Choi, V. V. Tsukruk, Graphene-polymer nanocomposites for structural and functional applications, *Prog. Polym. Sci.* 39 (2014) 1934–1972. <https://doi.org/https://doi.org/10.1016/j.progpolymsci.2014.03.001>.
- [5] M. Zhang, R.R. Parajuli, D. Mastrogiovanni, B. Dai, P. Lo, W. Cheung, R. Brukh, P.L. Chiu, T. Zhou, Z. Liu, E. Garfunkel, H. He, Production of Graphene Sheets by Direct Dispersion with Aromatic Healing Agents, *Small*. 6 (2010) 1100–1107. <https://doi.org/10.1002/smll.200901978>.
- [6] J. Minář, J. Brožek, ϵ -Caprolactone as a medium for improving dispersability of graphene oxide in polyamide based composites, *Eur. Polym. J.* 91 (2017) 212–220. <https://doi.org/https://doi.org/10.1016/j.eurpolymj.2017.03.058>.
- [7] A.A. Balandin, S. Ghosh, W. Bao, I. Calizo, D. Teweldebrhan, F. Miao, C.N. Lau, Superior Thermal Conductivity of Single-Layer Graphene, *Nano Lett.* 8 (2008) 902–907. <https://doi.org/10.1021/nl0731872>.
- [8] J.-U. Lee, D. Yoon, H. Kim, S.W. Lee, H. Cheong, Thermal conductivity of suspended pristine graphene measured by Raman spectroscopy, *Phys. Rev. B*. 83 (2011). <https://doi.org/10.1103/physrevb.83.081419>.
- [9] K.I. Bolotin, K.J. Sikes, Z. Jiang, M. Klima, G. Fudenberg, J. Hone, P. Kim, H.L. Stormer, Ultrahigh electron mobility in suspended graphene, *Solid State Commun.* 146 (2008) 351–355. <https://doi.org/https://doi.org/10.1016/j.ssc.2008.02.024>.
- [10] M.D. Stoller, S. Park, Y. Zhu, J. An, R.S. Ruoff, Graphene-Based Ultracapacitors, *Nano Lett.* 8 (2008) 3498–3502. <https://doi.org/10.1021/nl802558y>.
- [11] Y. Zhu, S. Murali, M.D. Stoller, K.J. Ganesh, W. Cai, P.J. Ferreira, A. Pirkle, R.M. Wallace, K.A. Cychosz, M. Thommes, D. Su, E.A. Stach, R.S. Ruoff, Carbon-based supercapacitors produced by activation of graphene, *Science* (80-.). 332 (2011) 1537–1541. <https://doi.org/10.1126/science.1200770>.
- [12] T. Dürkop, S.A. Getty, E. Cobas, M.S. Fuhrer, Extraordinary Mobility in Semiconducting Carbon Nanotubes, *Nano Lett.* 4 (2004) 35–39. <https://doi.org/10.1021/nl034841q>.
- [13] O.M. Istrate, K.R. Paton, U. Khan, A. O'Neill, A.P. Bell, J.N. Coleman, Reinforcement in melt-processed polymer-graphene composites at extremely low graphene loading level, *Carbon N. Y.* 78 (2014) 243–249. <https://doi.org/https://doi.org/10.1016/j.carbon.2014.06.077>.
- [14] G.M. Scheuermann, L. Rumi, P. Steurer, W. Bannwarth, R. Mülhaupt, Palladium Nanoparticles on Graphite Oxide and Its Functionalized Graphene Derivatives as Highly Active Catalysts for the Suzuki-Miyaura Coupling Reaction, *J. Am. Chem. Soc.* 131 (2009) 8262–8270. <https://doi.org/10.1021/ja901105a>.
- [15] L. Meda, G. Tozzola, A. Tacca, G. Marra, S. Caramori, V. Cristino, C. Alberto Bignozzi, Photoelectrochemical properties of nanostructured WO₃ prepared with different organic dispersing agents, *Sol. Energy Mater. Sol. Cells*. 94 (2010) 788–796. <https://doi.org/https://doi.org/10.1016/j.solmat.2009.12.025>.

- [16] D. Tasis, K. Papagelis, P. Spiliopoulos, C. Galiotis, Efficient exfoliation of graphene sheets in binary solvents, *Mater. Lett.* 94 (2013) 47–50. <https://doi.org/https://doi.org/10.1016/j.matlet.2012.12.027>.
- [17] J.-M. Malho, P. Laaksonen, A. Walther, O. Ikkala, M.B. Linder, Facile Method for Stiff, Tough, and Strong Nanocomposites by Direct Exfoliation of Multilayered Graphene into Native Nanocellulose Matrix, *Biomacromolecules.* 13 (2012) 1093–1099. <https://doi.org/10.1021/bm2018189>.
- [18] D. Han, L. Yan, W. Chen, W. Li, P.R. Bangal, Cellulose/graphite oxide composite films with improved mechanical properties over a wide range of temperature, *Carbohydr. Polym.* 83 (2011) 966–972. <https://doi.org/https://doi.org/10.1016/j.carbpol.2010.09.006>.
- [19] X. Wang, L. Zhi, K. Müllen, Transparent, Conductive Graphene Electrodes for Dye-Sensitized Solar Cells, *Nano Lett.* 8 (2008) 323–327. <https://doi.org/10.1021/nl072838r>.
- [20] R.J. Moon, A. Martini, J. Nairn, J. Simonsen, J. Youngblood, Cellulose nanomaterials review: structure, properties and nanocomposites, *Chem. Soc. Rev.* 40 (2011) 3941–3994. <https://doi.org/10.1039/C0CS00108B>.
- [21] D. Klemm, B. Heublein, H.-P.P. Fink, A. Bohn, Cellulose: Fascinating Biopolymer and Sustainable Raw Material, *Angew. Chemie Int. Ed.* 44 (2005) 3358–3393. <https://doi.org/10.1002/anie.200460587>.
- [22] O. Dahl, K. Vanhatalo, K. Parviainen, M. Svedman, A novel method to produce microcellulose, WO2011154601A1, 2011.
- [23] K.M. Vanhatalo, O.P. Dahl, Effect of Mild Acid Hydrolysis Parameters on Properties of Microcrystalline Cellulose, *BioResources.* 9 (2014) 4729–4740. https://ojs.cnr.ncsu.edu/index.php/BioRes/article/view/BioRes_09_3_4729_Vanhatalo_Mild_Acid_Hydrolysis_Parameters.
- [24] K. Dimic-Misic, K. Vanhatalo, O. Dahl, P. Gane, Rheological Properties Comparison of Aqueous Dispersed Nanocellulose Derived from a Novel Pathway-produced Microcrystalline Cellulose or by Conventional Methods, *Appl. Rheol.* 28 (2018). <https://doi.org/10.3933/applrheol-28-64474>.
- [25] M. Sasaki, B. Kabyemela, R. Malaluan, S. Hirose, N. Takeda, T. Adschiri, K. Arai, Cellulose hydrolysis in subcritical and supercritical water, *J. Supercrit. Fluids.* 13 (1998) 261–268. [https://doi.org/10.1016/S0896-8446\(98\)00060-6](https://doi.org/10.1016/S0896-8446(98)00060-6).
- [26] D.A. Cantero, M.D. Bermejo, M.J.J. Cocero, Kinetic analysis of cellulose depolymerization reactions in near critical water, *J. Supercrit. Fluids.* 75 (2013) 48–57. <https://doi.org/10.1016/j.supflu.2012.12.013>.
- [27] J. Buffiere, P. Ahvenainen, M. Borrega, K. Svedström, H. Sixta, Supercritical water hydrolysis: a green pathway for producing low-molecular-weight cellulose, *Green Chem.* 18 (2016) 6516–6525. <https://doi.org/10.1039/C6GC02544G>.
- [28] L.K. Tolonen, P.A. Penttilä, R. Serimaa, A. Kruse, H. Sixta, P.A. Penttilä, R. Serimaa, A. Kruse, H. Sixta, P.A. Penttilä, R. Serimaa, A. Kruse, H. Sixta, The swelling and dissolution of cellulose crystallites in subcritical and supercritical water, *Cellulose.* 20 (2013) 2731–2744. <https://doi.org/10.1007/s10570-013-0072-7>.
- [29] J. Buffiere, N. Abad, P. Ahvenainen, J. Dou, M.J. Cocero, H. Sixta, Tailoring the Structure and Morphology of Low-Molecular-Weight Cellulose Produced during Supercritical Water Hydrolysis, *ACS Sustain. Chem. Eng.* 6 (2018) 16959–16967. <https://doi.org/10.1021/acssuschemeng.8b04296>.
- [30] J. Buffiere, Z. Balogh-Michels, M. Borrega, T. Geiger, T. Zimmermann, H. Sixta, The chemical-free production of nanocelluloses from microcrystalline cellulose and their use as Pickering

- emulsion stabilizer, *Carbohydr. Polym.* 178 (2017) 48–56. <https://doi.org/10.1016/j.carbpol.2017.09.028>.
- [31] L. Nguyen Dang, J. Seppälä, Electrically conductive nanocellulose/graphene composites exhibiting improved mechanical properties in high-moisture condition, *Cellulose*. 22 (2015) 1799–1812. <https://doi.org/10.1007/s10570-015-0622-2>.
- [32] P. Sun, S. Kuga, M. Wu, Y. Huang, Exfoliation of graphite by dry ball milling with cellulose, *Cellulose*. 21 (2014) 2469–2478. <https://doi.org/10.1007/s10570-014-0264-9>.
- [33] J. Phiri, L. Johansson, P. Gane, T.C. Maloney, Co-exfoliation and fabrication of graphene based microfibrillated cellulose composites – mechanical and thermal stability and functional conductive properties, *Nanoscale*. 10 (2018) 9569–9582. <https://doi.org/10.1039/C8NR02052C>.
- [34] K. Dimic-Misic, J. Phiri, K. Nieminen, T. Maloney, P. Gane, Characterising exfoliated few-layer graphene interactions in co-processed nanofibrillated cellulose suspension via water retention and dispersion rheology, *Mater. Sci. Eng. B*. 242 (2019) 37–51. <https://doi.org/https://doi.org/10.1016/j.mseb.2019.03.001>.
- [35] M. -C. Yang, L.E. Scriven, C.W. Macosko, Some Rheological Measurements on Magnetic Iron Oxide Suspensions in Silicone Oil, *J. Rheol. (N. Y. N. Y)*. 30 (1986) 1015–1029. <https://doi.org/10.1122/1.549892>.
- [36] M. Mehrali, E. Sadeghinezhad, S.T. Latibari, S.N. Kazi, M. Mehrali, M.N.B.M. Zubir, H.S.C. Metselaar, Investigation of thermal conductivity and rheological properties of nanofluids containing graphene nanoplatelets, *Nanoscale Res. Lett.* 9 (2014) 15. <https://doi.org/10.1186/1556-276X-9-15>.
- [37] T. Moberg, K. Sahlin, K. Yao, S. Geng, G. Westman, Q. Zhou, K. Oksman, M. Rigdahl, Rheological properties of nanocellulose suspensions: effects of fibril/particle dimensions and surface characteristics, *Cellulose*. 24 (2017) 2499–2510. <https://doi.org/10.1007/s10570-017-1283-0>.
- [38] M. Mohtaschemi, K. Dimic-Misic, A. Puisto, M. Korhonen, T. Maloney, J. Paltakari, M.J. Alava, Rheological characterization of fibrillated cellulose suspensions via bucket vane viscometer, *Cellulose*. 21 (2014) 1305–1312. <https://doi.org/10.1007/s10570-014-0235-1>.
- [39] L.K. Tolonen, M. Juvonen, K. Niemelä, A. Mikkelsen, M. Tenkanen, H. Sixta, Supercritical water treatment for cello-oligosaccharide production from microcrystalline cellulose, *Carbohydr. Res.* 401 (2015) 16–23. <https://doi.org/10.1016/j.carres.2014.10.012>.
- [40] K. Dimic-Misic, A. Puisto, P. Gane, K. Nieminen, M. Alava, J. Paltakari, T. Maloney, The role of MFC/NFC swelling in the rheological behavior and dewatering of high consistency furnishes, *Cellulose*. 20 (2013) 2847–2861. <https://doi.org/10.1007/s10570-013-0076-3>.
- [41] K. Dimic-Misic, T. Maloney, P. Gane, Effect of fibril length, aspect ratio and surface charge on ultralow shear-induced structuring in micro and nanofibrillated cellulose aqueous suspensions, *Cellulose*. 25 (2018) 117–136. <https://doi.org/10.1007/s10570-017-1584-3>.
- [42] A.B. Fall, S.B. Lindström, O. Sundman, L. Ödberg, L. Wågberg, Colloidal stability of aqueous nanofibrillated cellulose dispersions, *Langmuir*. 27 (2011) 11332–11338. <https://doi.org/10.1021/la201947x>.
- [43] X. Sha, K. Yu, H. Cao, K. Qian, Shear thickening behavior of nanoparticle suspensions with carbon nanofillers, *J. Nanoparticle Res.* 15 (2013) 1816. <https://doi.org/10.1007/s11051-013-1816-x>.
- [44] N. Roussel, C. Lanos, Particle Fluid Separation in Shear Flow of Dense Suspensions: Experimental Measurements on Squeezed Clay Pastes, *Appl. Rheol.* 141410 (2004) 256–265. <https://doi.org/10.1515/arh-2004-0015>.
- [45] P. Coussot, Rheological Aspects of the Solid-Liquid Transition in Jammed Systems, in: M.C.

- Miguel, M. Rubi (Eds.), *Jamming, Yielding, Irreversible Deform. Condens. Matter*, Springer-Verlag, Berlin, Heidelberg, 2006: pp. 69–90. https://doi.org/10.1007/3-540-33204-9_5.
- [46] T. Divoux, C. Barentin, S. Manneville, From stress-induced fluidization processes to Herschel-Bulkley behaviour in simple yield stress fluids, *Soft Matter*. 7 (2011) 8409–8418. <https://doi.org/10.1039/C1SM05607G>.
- [47] H.J. Walls, S.B. Caines, A.M. Sanchez, S.A. Khan, Yield stress and wall slip phenomena in colloidal silica gels, *J. Rheol. (N. Y. N. Y)*. 47 (2003) 847–868. <https://doi.org/10.1122/1.1574023>.
- [48] M. Imani, A. Ghasemian, M.R. Dehghani-Firouzabadi, E. Afra, M. Borghei, L.S. Johansson, P.A.C. Gane, O.J. Rojas, Coupling Nanofibril Lateral Size and Residual Lignin to Tailor the Properties of Lignocellulose Films, *Adv. Mater. Interfaces*. 6 (2019) 1900770. <https://doi.org/10.1002/admi.201900770>.
- [49] M. Imani, A. Ghasemian, M.R. Dehghani-Firouzabadi, A. Elyas, P.A.C. Gane, O.J. Rojas, Nanolignocellulose from recycled fibres in coatings from aqueous and ethanolic media: effect of residual lignin on wetting and offset printing quality, *Nord. Pulp Pap. Res. J.* 34 (2019) 200. <https://doi.org/10.1515/npprj-2018-0053>.
- [50] Sunkyu Park, John O Baker, Michael E Himmel, Philip A Parilla, David K Johnson, Cellulose crystallinity index: measurement techniques and their impact on interpreting cellulase performance, *Biotechnol. Biofuels*. 3 (2010) 1–10. [http://www.biotechnologyforbiofuels.com/content/3/1/10%5Cnfile:///C:/Users/takehiko/Desktop/Cellulose crystallinity index_measurement techniques and their impact on interpreting cellulase performance.pdf](http://www.biotechnologyforbiofuels.com/content/3/1/10%5Cnfile:///C:/Users/takehiko/Desktop/Cellulose%20crystallinity%20index_measurement%20techniques%20and%20their%20impact%20on%20interpreting%20cellulase%20performance.pdf).
- [51] B. Lindman, B. Medronho, L. Alves, C. Costa, H. Edlund, M. Norgren, The relevance of structural features of cellulose and its interactions to dissolution, regeneration, gelation and plasticization phenomena, *Phys. Chem. Chem. Phys.* 19 (2017) 23704–23718. <https://doi.org/10.1039/c7cp02409f>.
- [52] R. Zheng, J. Gao, J. Wang, G. Chen, Reversible temperature regulation of electrical and thermal conductivity using liquid–solid phase transitions, *Nat. Commun.* 2 (2011) 289. <https://doi.org/10.1038/ncomms1288>.
- [53] M. Laka, S. Chernyavskaya, Obtaining microcrystalline cellulose from softwood and hardwood pulp, *BioResources*. 2 (2007) 583–589.
- [54] M.A. Hubbe, P. Tayeb, M. Joyce, P. Tyagi, M. Kehoe, K. Dimic-Misic, L. Pal, Rheology of Nanocellulose-rich Aqueous Suspensions: A Review, *Bioresources*. 12 (2017). https://ojs.cnr.ncsu.edu/index.php/BioRes/article/view/BioRes_12_4_9556_Hubbe_Rheology_Nanocellulose_Aqueous_Suspension.
- [55] R. Rahman, J. Foster, A. Haque, Molecular Dynamics Simulation and Characterization of Graphene-Cellulose Nanocomposites, *J. Phys. Chem. A*. 117 (2013). <https://doi.org/10.1021/jp402814t>.
- [56] W.J. Tseng, C.H. Wu, Aggregation, rheology and electrophoretic packing structure of aqueous Al₂O₃ nanoparticle suspensions, *Acta Mater.* 50 (2002) 3757–3766. [https://doi.org/https://doi.org/10.1016/S1359-6454\(02\)00142-8](https://doi.org/https://doi.org/10.1016/S1359-6454(02)00142-8).